High-field magnetoresistance of graphite revised

José Barzola-Quiquia,[1] Pablo D. Esquinazi,[1,*] Christian E. Precker,[1] Markus Stiller,[1] Mahsa Zoraghi,[1,†] Tobias Förster,[2] Thomas Herrmannsdörfer,[2] and William A. Coniglio[3]

[1]*Division of Superconductivity and Magnetism, Felix-Bloch-Institut für Festkörperphysik, Universität Leipzig, Linnéstrasse 5, D-04103 Leipzig, Germany*

[2]*Hochfeld-Magnetlabor Dresden (HLD-EMFL), Helmholtz-Zentrum Dresden-Rossendorf, D-01328 Dresden, Germany*

[3]*National High Magnetic Field Laboratory, 1800 East Paul Dirac Drive, Tallahassee, Florida 32310-3706, USA*

(Received 24 January 2019; published 17 May 2019)

A detailed magnetoresistance (MR) study of bulk and microflake samples of highly oriented pyrolytic graphite in a broad temperature $240 \gtrsim T \gtrsim 1$ K and magnetic field $\mu_0 H \leqslant 62$ T range, reveals the existence of three independent phenomena, the contributions of which are observed at different temperatures and fields. The identification of the three phenomena was possible by studying the MR of samples with thickness of 25 μm to 23 nm. At temperatures $T \gtrsim 100$ K the MR is mainly given by the semiconducting stacking order regions. At lower temperatures the contribution of the internal interfaces of graphite to its MR is clearly observable. These interfaces are the origin of the commonly observed electronic phase transitions at fields $35 \lesssim \mu_0 H \lesssim 55$ T at $T \lesssim 10$ K as well as a background MR in the whole field range that resembles the MR measured in granular superconductors.

DOI: 10.1103/PhysRevMaterials.3.054603

I. INTRODUCTION

In the early 1980s, Tanuma *et al.* reported a sharp increase in the magnetoresistance (MR) of graphite when a strong magnetic field $\mu_0 H \geqslant 20$ T is applied parallel to the c axis at temperatures $T < 10$ K [1]. Later, this observation was confirmed in different kinds of graphite samples, e.g., in Kish graphite [2–8], and synthesized as a byproduct in steelmaking and in highly oriented pyrolytic graphite (HOPG) [9–11]; for recent reviews, see Refs. [12,13]. There are a number of theoretical studies trying to provide an answer to several details of the electronic transitions observed in graphite at high fields and low temperatures. Yoshioka and Fukuyama [14], for example, proposed the existence of charge-density waves or spin-density waves to explain such electronic anomalies. Also, an excitonic BCS-like state was proposed to understand the behavior observed at fields above 50 T [3]. Recently, the field-induced metal-insulator transitions in thin flakes of Kish graphite with thickness $t = 178$ and 70 nm were studied [7], also under the influence of an electric field [8]. Those results were tentatively interpreted, suggesting that the electronic state in the insulating phase has an order along the stacking c-axis direction [8].

Several unclear experimental details of the field dependence of the electrical resistance of graphite samples added to the different interpretations demonstrate that there is no consent on the origin of the field-induced transitions. Part of the reason is related not only to details of the proposed phase diagram [12,13] but to conflicting experimental evidence, as, for example, that the electronic transitions are sometimes absent in certain ordered graphite samples [9,15]. This unclear conflicting evidence plus different sample dependent features published in the literature on the magnetoresistance of graphite in the last ten years suggest that these high-field transitions as well as the metal-insulator transition are not intrinsic of the graphite ideal structure. One of the main aims of our studies is to prove that the reported field-induced transitions are not intrinsic to the ideal graphite structure. Therefore, a relevant portion of the published interpretations must be revised.

II. THE INTERNAL STRUCTURE OF GRAPHITE SAMPLES: THE EXISTENCE OF INTERNAL INTERFACES

Earlier experimental studies reported the vanishing of the Shubnikov–de-Haas (SdH) oscillation amplitude the thinner the Kish graphite samples [16,17]. Furthermore, a nonlinear increase of the resistance of graphite samples by decreasing their thickness was reported [18], i.e., the absolute resistivity increases the thinner the sample [19,20]. Moreover, one of the apparently most robust properties of bulk graphite, its huge diamagnetic magnetization, was shown recently to depend also on the sample thickness [21]. All this experimental evidence is at odds with the hypothesis of homogeneity assumed in most of the investigations of the electronic transport properties of graphite and speaks to an unconventional contribution of interfaces embedded within a semiconducting matrix.

The recently published evidence on the thickness dependence of the galvanomagnetic behavior of a large number of graphite samples [20,22,23] indicates that several published features are related to internal two-dimensional (2D) interfaces. In other words, the measured electrical properties of

*esquin@physik.uni-leipzig.de

†Current address: Department of Neurophysics, Max Planck Institute for Human Cognitive and Brain Sciences, 04103 Leipzig, Germany.

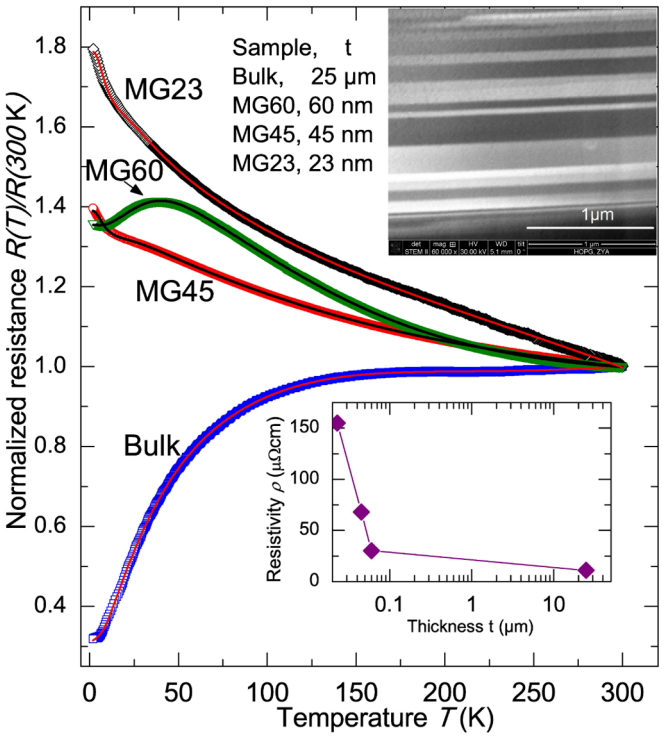

FIG. 1. Normalized resistance of the investigated samples vs temperature. The lines through the data points are fits to the three contributions in parallel as described in detail in Refs. [20,22,23]. The main change between the bulk and the thinner flakes is given by the weight of the metalliclike interfaces conductance. The inset at the bottom shows the resistivity as a function of the thickness t at room temperature. The upper inset shows a STEM image with the e beam parallel to the graphene planes of graphite. The c axis of the graphite structure is normal to the interfaces existing between crystalline regions, shown with different brightnesses. Those regions correspond either to crystalline Bernal regions twisted around the common c axis or to the rhombohedral phase. For further STEM pictures see Ref. [24].

graphite do not correspond to those of a homogeneous (structurally and electrically) graphite sample, whether the samples were natural graphite, HOPG, or Kish graphite [20,24].

Graphite is a layered material built by weakly coupled graphene sheets, where usually the graphene layers adopt a hexagonal *ABABA*... (2H) stacking sequence (Bernal) [25] or as a minority phase the *ABCABCA*... stacking order [rhombohedral (3R)] [26]. Scanning transmission electron microscopy (STEM) measurements show that most of the samples are formed by a stacking of crystalline blocks with well-defined interfaces between them (see the upper right inset in Fig. 1, as an example). One of the advantages of using HOPG of high grade to study the thickness dependence of the graphite properties is the fact that the density of interfaces (i.e., the number of interfaces per $\sim$1-μm-thick region parallel to the c axis of the graphite structure) is relatively constant, independently of the region of the sample that one cuts from the bulk HOPG piece. This knowledge comes from a large number of STEM images obtained in this graphite type, in clear contrast to natural graphite samples [27], for example.

Nevertheless, the characterization of single interfaces, even the knowledge of their lengths in the two directions (normal to the c axis) in samples of several-square-micrometers area (as our samples) or larger, cannot be simply obtained. The reason is that some of the 2D interfaces localized in depth of the usually measured TEM lamellas cannot appear with clear boundaries in the usual STEM pictures. Moreover, their lengths are smaller than the length of the graphene planes due to interface boundaries (see, e.g., Ref. [21]). Taking into account all the STEM pictures obtained in HOPG samples of grade A, we can state with certainty that the absolute number of interfaces decreases the thinner the sample but it does not necessarily decrease to zero. In other words, even in the case of a bilayer graphene sample, i.e., the thinnest sample possible with stacking *AB*, a twisted region can still exist in a several-square-micrometers-large area.

In general, three types of interfaces can be found, namely, between twisted 2H crystalline regions (we name it type I), between twisted 3R regions (type II), and between (twisted) 3R/2H regions (type III). The twist angle θ_t between the two crystalline regions of an interface is defined through a rotation around the common c axis (see, e.g., Ref. [24]). It may play a main role in the electronic properties of a given interface. For example, Van Hove singularities in the density of states are situated closer to the zero-bias energy at smaller θ_t [28], or a flat band is expected at $\theta_t = 0^\circ$ for a type-III interface [29,30]. The thickness of the crystalline regions (in the c-axis direction) having a common interface varies between ≈ 10 and 500 nm upon sample and the location within the same sample. Electron back scattering diffraction indicates that the lateral sizes of those crystalline regions in HOPG samples range between <3 and $\approx 20\,\mu$m [31]. This means that our microflake sizes are of the order of the crystal lateral size in HOPG.

We further note that superconductivity at $\sim$1 K was discovered in a single interface, a twisted bilayer graphene [32]. However, evidence for granular superconductivity with much higher critical temperatures at embedded interfaces in bulk HOPG and natural graphite samples was reported earlier [27,33–35]. Therefore, we expect that the main MR signal measured at low enough temperatures and thick enough graphite samples should be mainly related to the electronic systems within the 2D interfaces. To show this we have studied the in-plane MR under pulsed magnetic fields $\mu_0 H \leqslant 62$ T (applied parallel to the c axis) in four different samples with thickness at 23 nm $\leqslant t \leqslant 25\,\mu$m and lateral size from millimeters to below 10 μm, obtained from a millimeter-size HOPG sample from Advanced Ceramics (grade A). Our results and in particular the thickness dependence of the MR behavior help us to recognize the main contributions to the MR of graphite.

In Sec. III we describe the samples and further experimental details. The MR results under pulsed fields of four samples are presented in Sec. IV. Those measurements were accompanied by the temperature dependence of the resistance $R(T)$ and MR measurements under stationary magnetic fields to 18 T, which are shown in the Supplemental Material [36], which includes the results of two further graphite samples. We provide in Sec. V an interpretation of the behavior of the MR of graphite samples in the whole field and temperature range.

TABLE I. Summary of sample dimensions and the absolute resistance at 300 K. The number after the label "MG" of the multigraphene samples indicates the corresponding sample thickness in nm.

Sample name	Length l (m)	Width w (m)	Thickness t (m)	R (300 K) (Ω)
Bulk	0.0035	7×10^{-4}	2.5×10^{-5}	0.023
MG60	4×10^{-6}	7×10^{-6}	6×10^{-8}	2.926
MG45	4×10^{-6}	9×10^{-6}	4.5×10^{-8}	6.7
MG23	6×10^{-6}	8×10^{-6}	2.3×10^{-8}	50.7

III. EXPERIMENTAL DETAILS AND SAMPLES

The graphite microflakes were produced by a rubbing method described in a previous publication [19]. After patterning the electrodes geometry for the resistance measurements using electron-beam lithography, the voltage and input current electrodes on the samples were produced by sputtering of Cr/Au. Table I shows the dimensions of the four samples shown in the main paper. All samples were from the same bulk HOPG sample of grade A. All measurements were done in a four-probe configuration and magnetic fields were applied along the c-axis direction of the graphite structure. The temperature dependence of the resistance and the low-field MR were initially characterized using a commercial ^{4}He cryostat. The high magnetic field MR was measured at the high magnetic field laboratory in Dresden (to 62 T applied with a pulse length of ∼150 ms) and in Tallahassee (dc fields to 18 T) within the temperature range of 1.2 to 245 K. A lock-in amplifier (3.33 kHz) was used to measure the voltage during the rise and decay of the magnetic field. The applied currents varied between 5 and 10 μA to avoid self-heating effects.

In general, HOPG samples of grade A thicker than $\gtrsim$100 nm show transport properties similar to bulk graphite. With the exception of Refs. [7,8], most of the previous studies on the high-field MR of graphite were done on thicker samples of millimeter size [1–5,9,11,14]. Taking into account the internal structure of the graphite samples [22,24,31] (see inset in Fig. 1), we need to reduce the sample thickness to tens of nanometers and also the lateral size to a few micrometers in order to get electrical properties with a weaker contribution of the internal interfaces, i.e., nearer to the intrinsic properties of ideal single phase graphite.

IV. RESULTS

A. Temperature dependence of the resistance $R(T)$ of graphite samples with different thickness

Figure 1 shows the temperature dependence of the resistance $R(T)$ of all four samples without applied field. In the inset of Fig. 1 the resistivity ρ is plotted as a function of sample thickness t. The temperature dependence of the electrical resistance can be very well understood assuming the parallel contribution of semiconducting regions with both stable stacking orders and a metalliclike contribution from the interfaces [20,22,23], as shown by the fits to the data in Fig. 1. Whereas the resistance of the thickest sample shows the typical metalliclike behavior of bulk graphite, the $R(T)$ of the microflakes tends to a semiconductinglike behavior the smaller the sample thickness. The change from metalliclike to semiconductinglike behavior, decreasing sample thickness, is due to the reduction of the number of highly conducting 2D interfaces [20]. Obviously, the (low) field-induced metal-insulator transition does not occur in thin graphite samples. The $R(T)$ curves shown in Fig. 1, as well as those obtained in more than 20 samples from different origins and measured at different laboratories, can be very well described between 2 and 1100 K with a parallel resistor model [23]. The difference in the fit parameters of the four samples shown in Fig. 1 is mainly in the total conductance of the interfaces, decreasing the thinner the sample [20,23].

B. The magnetoresistance of the bulk sample

1. Evidence for a semiconducting behavior of the magnetoresistance at high enough temperatures

We now discuss the magnetoresistance, defined as MR = $[R(H) - R(0)]/R(0)$, at different temperatures shown in Fig. 2 for the bulk sample. In general, at $T \gtrsim 150$ K the contribution of the interfaces to the total MR starts to be overwhelmed by the higher conductance of the two semiconducting phases

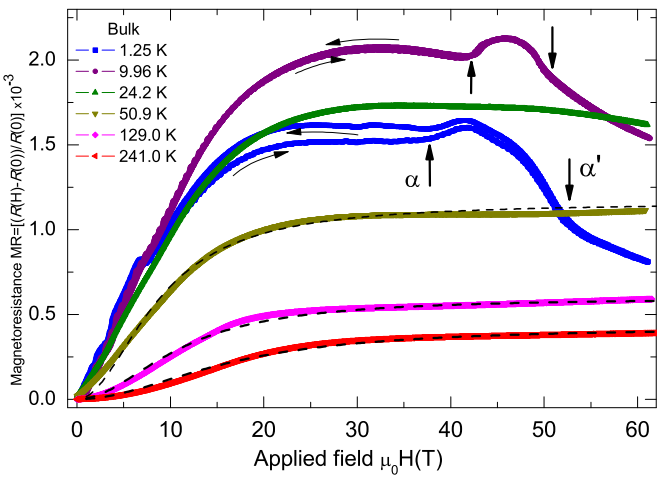

FIG. 2. High magnetic field results of the HOPG bulk sample ($t = 25\,\mu$m). The vertical arrows indicate the "critical fields" $\alpha(T)$ and $\alpha'(T)$. The horizontal arrows indicate the field sweep direction. The dashed lines through the data points at the three highest temperatures are fits to Eq. (1) with the parameters $\Delta n/n = 0.0484$ and $\mu = 1.277$ m^2/V s at $T = 241$ K. At lower T, μ slightly increases whereas $\Delta n/n$ decreases (see Supplemental Material [36] for a discussion of the parameters). The best possible fit of the data at 50.9 K to Eq. (1) is shown only to emphasize the disagreement at low fields and the develop of a maximum at ∼30 T. The fits to Eq. (1) get much worse at lower T.

contributing in parallel [23]. Therefore, at high enough temperatures the MR behaves as the one of a (low-gap) semiconductor. For graphite samples with lateral dimensions larger than the mean free path [31,37,38], the two-band model given by Eq. (1) and derived under the Boltzmann-Drude quasiclassical diffusive approach [39] provides a good (qualitative) description of the MR of bulk graphite at $T > 120\,\mathrm{K}$ (dashed lines in Fig. 2). The equation

$$\mathrm{MR} = \left[\mu^2 B^2 \left(1 - \frac{\Delta n^2}{n^2}\right)\right] \Big/ \left[1 + \mu^2 B^2 \frac{\Delta n^2}{n^2}\right] \qquad (1)$$

is a simplified version of the two-band model equation assuming equal mobility for both electrons and holes ($\mu = \mu_e \approx \mu_h$), with $\Delta n/n = (n_e - n_h)/(n_e + n_h)$ the relative charge imbalance between electron n_e and hole n_h carrier densities and $B = \mu_0 H$. This simplified expression has only two adjustable fitting parameters, the average mobility μ and the relative charge imbalance $\Delta n/n$, and it is insensitive to the absolute value of n_e (or n_h). Equation (1) provides two key features of the experimental MR, namely, the B^2 field dependence at low fields and its saturation at high enough fields (see Fig. 2). Note that the parameters obtained from the fit of the MR to Eq. (1) are not related to the ones obtained from the SdH oscillations because they belong to two different electronic systems. Namely, the semiconducting behavior is due to the graphite regions without interfaces, whereas the 2D electronic systems, the origin of the SdH oscillations, are localized at the 2D interfaces [20,22,23].

2. Negative magnetoresistance and electronic transitions at low temperatures and high enough fields

The MR data at $T \leqslant 50.9\,\mathrm{K}$ shown in Fig. 2 deviate from the predictions of the two-band model [independently of the fitting parameters used in Eq. (1)]: there is a linear field dependence at low fields and a maximum around 30 T develops. The negative MR at high fields becomes more pronounced the lower the temperature and, in addition, a clear bump between ≈ 35 and ≈ 55 T appears. This behavior has been reported for Kish and HOPG graphite and it was attributed to field-induced phase transitions at T-dependent critical fields $\alpha(T)$ and $\alpha'(T)$ (indicated by vertical arrows in Fig. 2) [4,6,9,12,13]. We further note that the overall MR decreases at $T < 10\,\mathrm{K}$. Also the absolute value of the resistance at high enough fields steadily decreases, i.e., R (1.25 K, 60 T) $\simeq 6\,\Omega < R$ (241 K, 60T) $\simeq 9\,\Omega$ (see Fig. S8 in Supplemental Material [36]). This is attributed to the so-called reentrance to a metallic state in the quantum limit, originally shown and discussed in Ref. [40].

At low temperatures, a hysteresis in the MR emerges at ≈ 12 T and vanishes at ≈ 50 T, the MR being smaller at the increasing field branch (see Fig. 2). The opening of a hysteresis at high fields was first mentioned by Takashi *et al.* [1] and further discussed in Ref. [41] using data from a Tanzanian natural graphite sample. We stress that such hysteresis in the MR is observed only at low temperatures and only in thick enough samples (see also Fig. 3). See Supplemental Material [36] for more details on the mentioned hysteresis.

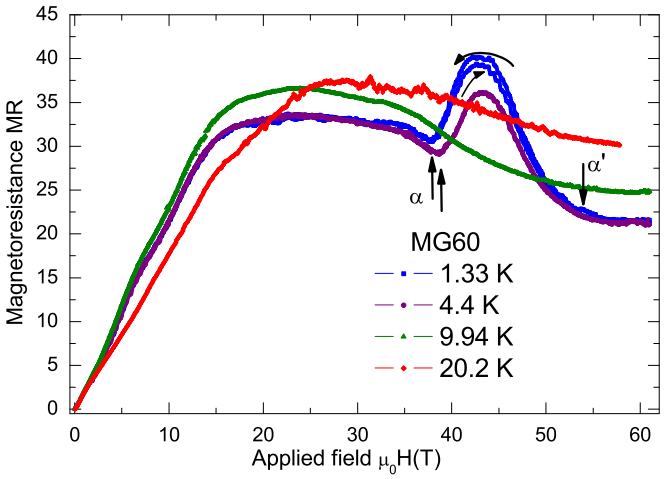

FIG. 3. High magnetic field magnetoresistance MR of sample MG60 at different temperatures. The vertical arrows indicate the critical fields $\alpha(T)$ and $\alpha'(T)$ and the horizontal arrows refer to the field sweep direction to emphasize the hysteresis observed only at the lowest temperature. At all other temperatures the curves are reversible in field within experimental resolution.

C. The magnetoresistance of the multigraphene samples

1. The magnetoresistance of the 60-nm-thick sample

We discuss the results of the thinner flakes. The MR results of sample MG60 are plotted in Fig. 3. One can clearly recognize the transitions at $\alpha(T)$ and $\alpha'(T)$. In general, the MR of this sample changes only slightly in the measured temperature range and behaves qualitatively similar to the bulk sample, in spite of two to three orders of magnitude smaller sample width, length, and thickness (see Table I). However, the MR is approximately two orders of magnitude smaller than in the bulk sample. We note that the decrease of the lateral size produces only a small reduction of the MR, compared to the bulk sample [31]. This indicates that the largest decrease of the MR is due to the decrease in the thickness and consequently in the amount of interfaces, as has been recently shown in a systematic study [20]. As in the bulk sample, a clear negative MR starts to appear at fields above $\sim$30 T and the field dependence is linear at low fields.

2. The magnetoresistance of the 45-nm-thick sample: First hints for a vanishing of the high-field electronic transitions

Results of sample MG45 are plotted in Fig. 4. In contrast to the previous samples, no evident field transition $\alpha(T)$ is observed. At the lowest temperature we can recognize a α' transition only. In the field range between 30 and 62 T and increasing T we observe a change from a negative to a positive MR. Note that the MR increases with T, without any sign of saturation at high fields, in clear contrast to the bulk sample. The MR is reversible within experimental resolution.

3. The magnetoresistance of the 23-nm-thick sample: Huge decrease of the overall MR and the vanishing of the high-field electronic transitions

The results of the thinnest sample MG23 are shown in Fig. 5. Its MR is overall much smaller than in the other

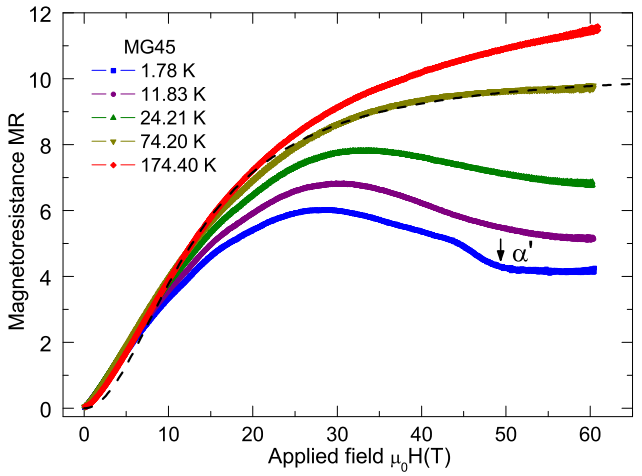

FIG. 4. High magnetic field magnetoresistance MR of sample MG45 ($t = 45$ nm) at different temperatures. The vertical arrow indicates the critical field $\alpha'(T = 1.78\ \mathrm{K})$. The dashed line is calculated from Eq. (1) to fit the high-field MR data at 74.20 K, for example, although this equation is not really applicable due to nondiffusive ballistic contribution (see text). Further, note the deviation of the data from the expected H^2 dependence at fields below 5 T.

samples and, as in sample MG45, its MR increases with temperature with no sign of saturation. As in the other samples, at low enough T and fields above 30 T, a negative MR is observed to 50 T. The MR of this sample shows only a smooth feature between 40 and 50 T, i.e., where the high-field-induced transitions were observed in the other samples, and at the lowest temperature.

V. DISCUSSION

In what follows we provide an interpretation of the main results. We note that due to the different, partially unknown, parallel contributions to the MR (one from the interfaces, which includes different types, and from the semiconducting layers [20,22,23]), the qualitative description we provide below uses the fact that the interfacial contribution to the

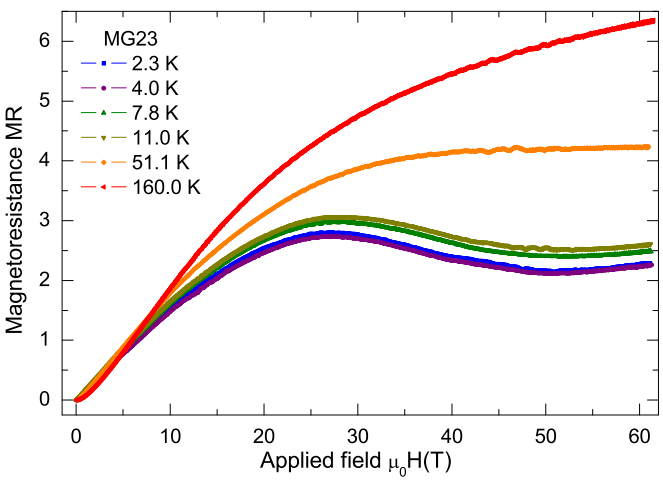

FIG. 5. High magnetic field MR of sample MG23 ($t =$ 23 nm ~80 graphene layers) at different temperatures.

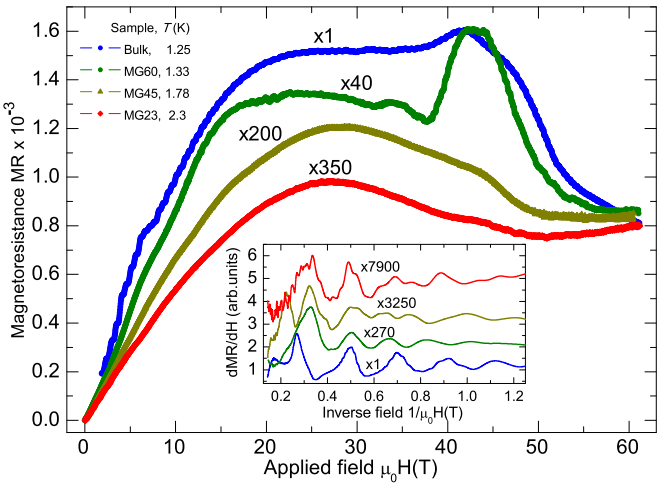

FIG. 6. Magnetoresistance of all samples investigated in this paper at the lowest temperature. The inset shows the SdH oscillations obtained at $T = 5$ K. The numbers beside the curves are the multiplication factors to show the results in the same scale.

total conductance overwhelms the other two at $T < 100$ K [23]. However, its influence on the MR weakens with fewer interfaces, as expected.

A. The main changes in the MR due to the decrease in the number of interfaces

The fact that the field-induced transitions at the fields $\alpha(T)$ and $\alpha'(T)$ systematically vanish the smaller the thickness of the samples (for similar lateral sample dimensions) indicates that these are not intrinsic of the ideal graphite structure. Taking into account previous galvanomagnetic studies [19,20,22–24], their suppression is related to the smaller number of certain internal interfaces. Our results and interpretation provide an answer to the absence of high-field electronic phase transitions in certain graphite samples mentioned in Refs. [9,15] as well as the scattering of the "critical fields" data.

The vanishing of the field-induced transitions is accompanied by a large decrease in the absolute MR in the whole field range (see Fig. 6). The decrease in the MR by a factor ~700 between the bulk and MG23 samples is mainly related to the decrease in the amount of interfaces.

The low-temperature MR curves in Fig. 6 suggest that the field-induced transitions are superposed to a MR curve that resembles that of the thinnest MG23 sample, i.e., the MR increases linearly in field at low fields, it reaches a maximum at $20 < \mu_0 H < 30$ T; and it shows a negative MR at $30 < \mu_0 H < 50$ T (see also Fig. 7). This fact added to the clear deviation from the expected two-band model behavior given by Eq. (1) suggests that even the behavior of the thinnest sample MG23 at low temperatures is not yet intrinsic of the graphite ideal structure. As a further proof of this interpretation, we note that the SdH oscillations measured in graphite samples are not intrinsic but related to the electronic 2D systems localized at certain interfaces [20]; these are observed in all samples (see inset in Fig. 6).

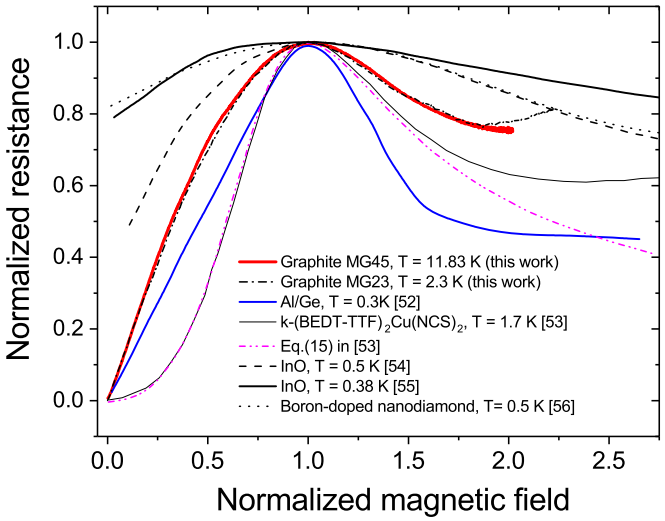

FIG. 7. Normalized resistance vs normalized magnetic field at different constant temperatures of graphite MG45 and MG23 samples measured in this paper, with the normalization field factor at resistance maximum of $\mu_0 H^\star = 27.5$ and 30 T at 11.83 and 2.3 K, respectively; the granular superconductor Al/Ge from Ref. [52] with $\mu_0 H^\star \simeq 2.3$ T at 0.3 K; the organic layered superconductor κ-(BEDT-TTF)$_2$Cu(NCS)$_2$ from Ref. [53] with $\mu_0 H^\star \simeq 2.8$ T at 1.7 K with the voltage measured parallel to the applied field; a granular superconducting InO thin film from Ref. [54] with $\mu_0 H^\star \simeq 2.4$ T at 0.5 K; InO thin film from Ref. [55] with $\mu_0 H^\star \simeq 3.0$ T at 0.38 K; and boron-doped nanocrystalline diamond film with $\mu_0 H^\star \simeq 1.4$ T at 0.5 K (sample q_2 from Ref. [56]).

Note, however, the decrease of the amplitude of the SdH oscillations (characterized by the first field derivative of the MR) is more than ten times larger than the decrease in the MR itself, suggesting that the MR of the graphite samples results from contributions of different interfaces or different regions within the same interfaces. A considerable amount of extensive experimental work needs to be done to characterize the contribution(s) of each kind of interfaces to the total MR.

B. Increase of the overall MR with temperature: Influence of the ballistic regime

Earlier experiments in thin graphite samples with no or a low number of interfaces showed that the mean free path of the carriers within the graphene layers can be several microns large [37], of the order of our sample lateral size. In this case a ballistic, not the diffusive regime assumed in Eq. (1), should be taken into account to understand the nonsaturation of the MR at high fields observed in the MG45 and MG23 samples (Figs. 4 and 5). The increase of the MR with temperature at all fields, as in the thinner samples MG45 and MG23, is observed because the carrier mean free path, of the order of the sample lateral size, decreases with temperature [31,37].

C. Influence of granular superconductivity

Current-voltage characteristic curves and the obtained Josephson-like critical current magnetic field response [42] as well as Shapiro-steps-like behavior of annealed graphite powders under radiation of 10 GHz [43] provided the first hints for the existence of granular superconductivity at certain regions of the graphite samples and at a surprisingly high temperature of 300 K. Magnetization measurements done in water-treated highly pure graphite powder [44] and in bulk HOPG samples confirmed the granular superconductivity behavior and its relation to the internal interfaces [45]. Hints for high-temperature superconductivity in graphite flakes embedded in alkanes were also reported [46]. The systematic studies done in different graphite samples in recent years indicate that certain interfaces in the graphite structure can have granular superconducting properties in a broad temperature range, i.e., from a few degrees Kelvin as in bilayer graphene [32], ≈ 3 K in low grade HOPG samples [35], ≈ 14 K at the surface of grafoil [47], up to ≈ 150 K in certain TEM lamellas prepared from HOPG grade A [33], or above room temperature in different HOPG, natural graphite, and finely ground pyrolytic graphite samples [27,48]. For further reading see Refs. [24,49,50] and references therein. We note also that the transition observed in bilayer graphene [32] may also indicate the existence of granular superconductivity as was recently pointed out by one of the authors [51]. Furthermore, the transitions shown in some of the other reports, e.g., Ref. [33], do not represent the intrinsic superconducting transition of the superconducting grains but the temperature at which the Josephson coupling between the regions gets robust enough to enable a large voltage drop at the input current path.

In this section we would like to discuss to what extent the high-field magnetoresistance provides some hints compatible with the existence of granular superconductivity localized at certain graphite interfaces of our samples. We propose that the main behavior of the MR shown in Fig. 6, i.e., the linear MR at low fields as well as the negative MR at $30 < \mu_0 H < 50$ T (a key feature of the high magnetic field results), is due to the magnetic field response of certain superconducting regions localized at interfaces of the graphite samples and it is not an intrinsic property of the ideal graphite stacking orders. We compare below our MR data with those obtained in granular superconductors at temperatures and fields below the critical values and in one case above the critical field.

In Fig. 7 we show the normalized MR data of the thinnest samples MG45 and MG23 at 11.83 and 2.3 K and include the MR data of granular Al in a Ge matrix from Ref. [52], obtained at 0.3 K. It is remarkable that the normalized MR data of our MG45 and MG23 samples are practically identical, pointing to a common origin. The MR data of granular Al/Ge show a linear field dependence at low fields and a clear negative MR in a field range comparable (in normalized units) to that of the graphite samples. In the case of granular Al/Ge the field at which the negative MR region ends is considered as the upper critical field of the superconducting grains at $\mu_0 H_{c2}$ (0.3 K) $\simeq 4.5$ T. In the case of the insulatinglike granular InO thin films [54,55] and boron-doped nanodiamond film [56], a similar behavior is observed (i.e., a linear increase with field below the maximum and a clear negative MR above it) although the negative MR field range has a larger normalized field extension. Note that in all granular superconducting examples and whether or not there is percolation (i.e., zero or finite resistance at zero field) the MR increases linearly with field (see Fig. 7).

The interpretation of the whole field behavior of the MR of granular superconductors can be divided into three field regimes. At fields below the maximum of the MR, the MR increases linearly with field due to the influence of the field on the Josephson coupling between the superconducting regions, i.e., a linear-in-field decrease of the total coupled regions. When the number and/or size of the superconducting regions increases, the increase with field of the MR gets more significant, as it is observed the lower the temperature. The linear-in-field behavior of the MR (at low fields) turns to a quadratic one the higher the temperature (see, for example, Figs. 2 and 4). The reason for this change is the overwhelming contribution of the semiconducting paths to the total conductance the higher the temperature, and not necessarily due to a change of the behavior of the interfaces themselves. Future experiments should try to measure the contribution of the interfaces to the MR, contacting them at the edges, as done in Ref. [33], reducing partially the relative contribution to the total conductance of the semiconducting regions in parallel. In this case we may have the possibility to check whether the MR behavior of the interfaces (represented by the normalized curves of samples MG45 and MG23 in Fig. 7) is still observable above 100 K.

We note that the maximum in the MR shows larger values of the resistance than in the normal state at the same temperature, which is reached at high enough fields. This fact as well as the negative MR observed above the maximum were explained in terms of granular superconductivity [52,55–57]. At sufficiently high magnetic fields Cooper pair transfer between the Josephson-coupled regions is suppressed and single-particle tunneling sets in. The negative MR is interpreted therefore as due to the reduction with field of the resistance between the superconducting regions. This happens when superconducting fluctuations (in terms of virtual Cooper pairs) affect the density of states of the tunneling quasiparticles. In other words the intragrain superconducting fluctuation affects the intergrain conductivity, producing a reduction of the total resistance at high enough fields. The differences in the behavior depicted by the normalized curves of Fig. 7 may be related to differences in grain size, grain coupling, and temperature.

The effect of superconducting fluctuations above the critical temperature and field have been studied in detail in recent years (see Ref. [58] and references therein). As an example, we include in Fig. 7 the MR data obtained from the layered organic superconductor κ-(BEDT-TTF)$_2$Cu(NCS)$_2$ at 1.7 K with the theoretical line given in Ref. [53]. One main difference with respect to the other data shown in that figure is that the MR follows a quadratic instead of a linear field dependence at low fields. The theory [53], therefore, is only applicable in the normal state of a granular superconductor.

From all the evidence obtained during the last years in graphite, it is plausible to assume that the temperatures where the maximum in the MR is observed are below the critical temperature of the superconducting grains. We assume that the field at which the negative MR ends (in Al/Ge that would be $\sim$1.8 times the field at the maximum MR) can be considered as a field near the critical field, i.e., $\mu_0 H_{c2}(0) \gtrsim 60$ T for the superconducting 2D regions at certain interfaces of graphite. Finally, we note that the MR oscillations periodic in field and the behavior under a bias voltage recently reported in thin graphite samples [8] were already observed earlier and their origins are also related to the existence of 2D interfaces and granular superconductivity [59,60].

VI. CONCLUSION

Magnetoresistance measurements of graphite samples of different thickness in a wide temperature and field range indicate that the reported field-induced electronic phase transitions are not intrinsic of the ideal graphite structure but related to 2D electronic systems localized at certain interfaces formed between the crystalline regions, commonly found in graphite samples with thickness above a few tens of nanometers. Our conclusion is also supported by the thickness dependence observed in other galvanomagnetic characterizations. We encourage the scientific community to revise the theoretical interpretations of the high-field transitions published in the past and to take into account explicitly the different kinds of possible interfaces graphite samples have.

ACKNOWLEDGMENTS

We gratefully acknowledge A. Gerber (Tel Aviv University) and A. A. Varlamov (Istituto Superconducttori, Rome) for useful discussions on granular superconductivity and fluctuation effects, and P. K. Muduli for discussion on the two-band model. C.E.P. gratefully acknowledges the support provided by the Brazilian National Council for the Improvement of Higher Education (CAPES) under Grant No. 99999.013188/2013-05. The studies were supported by German Academic Exchange Service (DAAD) Grant No. 57207627 (“Untersuchungen von Grenzflächen in Graphit bei sehr hohen Feldern”) and partially supported by the German Research Foundation (DFG) under Grants No. ES 86/29-1 and No. SFB 762. A portion of this work was performed at the National High Magnetic Field Laboratory, which is supported by National Science Foundation Cooperative Agreement No. DMR- 1157490 and the State of Florida. We acknowledge the support of the HLD at HZDR, member of the European Magnetic Field Laboratory.

[1] S. Tanuma, R. Inada, A. Furukawa, O. Takahashi, and Y. Iye, *Physics in High Magnetic Fields* (Springer, Berlin, 1981), p. 316.
[2] H. Yaguchi and J. Singleton, Phys. Rev. Lett. **81**, 5193 (1998).
[3] K. Akiba, A. Miyake, H. Yaguchi, A. Matsuo, K. Kindo, and M. Tokunaga, J. Phys. Soc. Jpn. **84**, 054709 (2015).
[4] S. Uji, J. S. Brooks, and Y. Iye, Physica B: Cond. Matt. **246–247**, 299 (1998).
[5] G. Timp, P. D. Dresselhaus, T. C. Chieu, G. Dresselhaus, and Y. Iye, Phys. Rev. B **28**, 7393(R) (1983).
[6] B. Fauqué, D. LeBoeuf, B. Vignolle, M. Nardone, C. Proust, and K. Behnia, Phys. Rev. Lett. **110**, 266601 (2013).

[7] T. Taen, K. Uchida, and T. Osada, Phys. Rev. B **97**, 115122 (2018).

[8] T. Taen, K. Uchida, T. Osada, and W. Kang, Phys. Rev. B **98**, 155136 (2018).

[9] Y. Iye, P. M. Tedrow, G. Timp, M. Shayegan, M. S. Dresselhaus, G. Dresselhaus, A. Furukawa, and S. Tanuma, Phys. Rev. B **25**, 5478 (1982).

[10] Y. Iye, M. Berglund, and L. E. McNeil, Solid State Commun. **52**, 975 (1984).

[11] Y. Kopelevich, B. Raquet, M. Goiran, W. Escoffier, R. R. da Silva, J. C. Medina Pantoja, I. A. Lukyanchuk, A. Sinchenko, and P. Monceau, Phys. Rev. Lett. **103**, 116802 (2009).

[12] H. Yaguchi and J. Singleton, J. Phys.: Condens. Matter **21**, 344207 (2009).

[13] B. Fauqué and K. Behnia, in *Basic Physics of Functionalized Graphite*, edited by P. D. Esquinazi (Springer, New York, 2016), Chap. 4, pp. 77–96.

[14] D. Yoshioka and H. Fukuyama, J. Phys. Soc. Jpn. **50**, 725 (1981).

[15] N. B. Brandt, G. A. Kapustin, V. G. Karavaev, A. S. Kotosonov, and E. A. Svistova, Zh. Eksp. Teor. Fiz. **67**, 1136 (1974) [Sov. Phys.-JETP **40**, 564 (1975)].

[16] Y. Ohashi, T. Hironaka, T. Kubo, and K. Shiiki, TANSO **195**, 410 (2000).

[17] Y. Ohashi, K. Yamamoto, and T. Kubo, in *Carbon'01, An International Conference on Carbon, Lexington, KY, United States, July 14–19* (American Carbon Society, 2001), p. 568, available at https://acs.omnibooksonline.com/.

[18] Y. Zhang, J. P. Small, W. V. Pontius, and P. Kim, Appl. Phys. Lett. **86**, 073104 (2005).

[19] J. Barzola-Quiquia, J.-L. Yao, P. Rödiger, K. Schindler, and P. Esquinazi, Phys. Status Solidi A **205**, 2924 (2008).

[20] M. Zoraghi, J. Barzola-Quiquia, M. Stiller, P. D. Esquinazi, and I. Estrela-Lopis, Carbon **139**, 1074 (2018).

[21] B. Semenenko and P. D. Esquinazi, Magnetochemistry **4**, 52 (2018).

[22] N. García, P. Esquinazi, J. Barzola-Quiquia, and S. Dusari, New J. Phys. **14**, 053015 (2012).

[23] M. Zoraghi, J. Barzola-Quiquia, M. Stiller, A. Setzer, P. Esquinazi, G. H. Kloess, T. Muenster, T. Lühmann, and I. Estrela-Lopis, Phys. Rev. B **95**, 045308 (2017).

[24] P. D. Esquinazi and Y. Lysogorskiy, in *Basic Physics of Functionalized Graphite*, edited by P. D. Esquinazi (Springer, New York, 2016), Chap. 7, pp. 145–179.

[25] J. D. Bernal, Proc. R. Soc. A **106**, 749 (1924).

[26] H. Lipson and A. R. Stokes, Proc. R. Soc. A **181**, 101 (1942).

[27] C. E. Precker, P. D. Esquinazi, A. Champi, J. Barzola-Quiquia, M. Zoraghi, S. Muiños-Landin, A. Setzer, W. Böhlmann, D. Spemann, J. Meijer, T. Muenster, O. Baehre, G. Kloess, and H. Beth, New J. Phys. **18**, 113041 (2016).

[28] I. Brihuega, P. Mallet, H. González-Herrero, G. Trambly de Laissardière, M. M. Ugeda, L. Magaud, J. M. Gómez-Rodríguez, F. Ynduráin, and J.-Y. Veuillen, Phys. Rev. Lett. **109**, 196802 (2012).

[29] W. A. Muñoz, L. Covaci, and F. M. Peeters, Phys. Rev. B **87**, 134509 (2013).

[30] N. B. Kopnin and T. T. Heikkilä, *Carbon-Based Superconductors: Towards High-T_c Superconductivity* (CRC, Boca Raton, FL, 2015), Chap. 9, pp. 231–263.

[31] J. C. Gonzalez, M. Muñoz, N. García, J. Barzola-Quiquia, D. Spoddig, K. Schindler, and P. Esquinazi, Phys. Rev. Lett. **99**, 216601 (2007).

[32] Y. Cao, V. Fatemi, S. Fang, K. Watanabe, T. Taniguchi, E. Kaxiras, and P. Jarillo-Herrero, Nature (London) **556**, 43 (2018).

[33] A. Ballestar, J. Barzola-Quiquia, T. Scheike, and P. Esquinazi, New J. Phys. **15**, 023024 (2013).

[34] A. Ballestar, T. T. Heikkilä, and P. Esquinazi, Superc. Sci. Technol. **27**, 115014 (2014).

[35] A. Ballestar, P. Esquinazi, and W. Böhlmann, Phys. Rev. B **91**, 014502 (2015).

[36] See Supplemental Material at http://link.aps.org/supplemental/10.1103/PhysRevMaterials.3.054603 for 7 figures, also with data from two new samples. The following sections are included: Temperature and field dependence of the resistance under DC magnetic fields to 18T; The reentrance to a metalliclike state at high magnetic fields in thick graphite samples; Parameters of the two-band model; The hysteresis in the magnetoresistance.

[37] S. Dusari, J. Barzola-Quiquia, P. Esquinazi, and N. García, Phys. Rev. B **83**, 125402 (2011).

[38] P. Esquinazi, J. Barzola-Quiquia, S. Dusari, and N. García, J. Appl. Phys. **111**, 033709 (2012).

[39] B. T. Kelly, *Physics of Graphite* (Applied Science, London, 1981).

[40] Y. Kopelevich, J. H. S. Torres, R. R. da Silva, F. Mrowka, H. Kempa, and P. Esquinazi, Phys. Rev. Lett. **90**, 156402 (2003).

[41] F. Arnold, A. Isidori, E. Kampert, B. Yager, M. Eschrig, and J. Saunders, Phys. Rev. Lett. **119**, 136601 (2017).

[42] K. Antonowicz, Nature (London) **247**, 358 (1974).

[43] K. Antonowicz, Phys. Status Solidi A **28**, 497 (1975).

[44] T. Scheike, W. Böhlmann, P. Esquinazi, J. Barzola-Quiquia, A. Ballestar, and A. Setzer, Adv. Mater. **24**, 5826 (2012).

[45] T. Scheike, P. Esquinazi, A. Setzer, and W. Böhlmann, Carbon **59**, 140 (2013).

[46] Y. Kawashima, AIP Advances **3**, 052132 (2013).

[47] F. Arnold, J. Nyéki, and J. Saunders, JETP Lett. **107**, 577 (2018).

[48] M. Saad, I. F. Gilmutdinov, A. G. Kiiamov, D. A. Tayurskii, S. I. Nikitin, and R. V. Yusupov, JETP Lett. **107**, 37 (2018).

[49] P. D. Esquinazi, C. E. Precker, M. Stiller, T. R. S. Cordeiro, J. Barzola-Quiquia, A. Setzer, and W. Böhlmann, Quantum Stud. Math. Found. **5**, 41 (2018).

[50] G. E. Volovik, JETP Lett. **107**, 516 (2018).

[51] P. D. Esquinazi, Ordered defects: A roadmap towards room temperature superconductivity and magnetic order, arXiv:1902.07489.

[52] A. Gerber, A. Milner, G. Deutscher, M. Karpovsky, and A. Gladkikh, Phys. Rev. Lett. **78**, 4277 (1997).

[53] A. Glatz, A. A. Varlamov, and V. M. Vinokur, Phys. Rev. B **84**, 104510 (2011).

[54] Y. Lee, A. Frydman, T. Chen, B. Skinner, and A. M. Goldman, Phys. Rev. B **88**, 024509 (2013).

[55] V. F. Gantmakher, M. V. Golubkov, J. G. S. Lok, and A. K. Geim, Zh. Eksp. Teor. Fiz. **109**, 1765 (1996) [JETP **82**, 951 (1996)].

[56] B. L. Willems, G. Zhang, J. Vanacken, V. V. Moshchalkov, S. D. Janssens, K. Haenen, and P. Wagner, J. Phys. D **43**, 374019 (2010).

[57] I. S. Beloborodov and K. B. Efetov, Phys. Rev. Lett. **82**, 3332 (1999).

[58] A. A. Varlamov, A. Galda, and A. Glatz, Rev. Mod. Phys. **90**, 015009 (2018).

[59] P. Esquinazi, N. García, J. Barzola-Quiquia, P. Rödiger, K. Schindler, J.-L. Yao, and M. Ziese, Phys. Rev. B **78**, 134516 (2008).

[60] A. Ballestar, P. Esquinazi, J. Barzola-Quiquia, S. Dusari, F. Bern, R. da Silva, and Y. Kopelevich, Carbon **72**, 312 (2014).